*Published online 17 June 2021*

*NAR Cancer, 2021, Vol. 3, No. 2* **1**
*https://doi.org/10.1093/narcan/zcab023*

# EVI1 activates tumor-promoting transcriptional enhancers in pancreatic cancer

**Hwa-Ryeon Kim[1,†], Juhye Yim[1,†], Hye-Been Yoo[1], Seung Eon Lee[1], Sumin Oh[2], Sungju Jung[2], Chang-il Hwang[3], Dong-Myung Shin[4,5], TaeSoo Kim[6], Kyung Hyun Yoo[2], You-Sun Kim[7,8], Han-Woong Lee[1] and Jae-Seok Roe[1,*]**

[1]Department of Biochemistry, Yonsei University, Seoul 03722, South Korea, [2]Department of Biological Sciences, Sookmyung Women's University, Seoul 04310, South Korea, [3]Department of Microbiology and Molecular Genetics, College of Biological Sciences, University of California, Davis, Davis, CA 95616, USA, [4]Department of Biomedical Sciences, Asan Medical Center, University of Ulsan College of Medicine, Seoul 05505, South Korea, [5]Department of Physiology, University of Ulsan College of Medicine, Seoul 05505, South Korea, [6]Department of Life Science and the Research Center for Cellular Homeostasis, Ewha Womans University, Seoul 03760, South Korea, [7]Department of Biochemistry, School of Medicine, Ajou University, Suwon 16499, South Korea and [8]Department of Biomedical Sciences, Graduate School, Ajou University, Suwon 16499, South Korea

Received March 11, 2021; Revised May 21, 2021; Editorial Decision May 27, 2021; Accepted May 28, 2021

## ABSTRACT

**Cancer cells utilize epigenetic alterations to acquire autonomous capabilities for tumor maintenance. Here, we show that pancreatic ductal adenocarcinoma (PDA) cells utilize super-enhancers (SEs) to activate the transcription factor EVI1 (ecotropic viral integration site 1) gene, resulting in activation of an EVI1-dependent transcription program conferring PDA tumorigenesis. Our data indicate that SE is the vital *cis*-acting element to maintain aberrant EVI1 transcription in PDA cells. Consistent with disease progression and inferior survival outcomes of PDA patients, we further show that EVI1 upregulation is a major cause of aggressive tumor phenotypes. Specifically, EVI1 promotes anchorage-independent growth and motility *in vitro* and enhances tumor propagation *in vivo*. Mechanistically, EVI1-dependent activation of tumor-promoting gene expression programs through the stepwise configuration of the active enhancer chromatin attributes to these phenotypes. In sum, our findings support the premise that EVI1 is a crucial driver of oncogenic transcription programs in PDA cells. Further, we emphasize the instructive role of epigenetic aberrancy in establishing PDA tumorigenesis.**

## INTRODUCTION

Pancreatic ductal adenocarcinoma (PDA) is one of the most common and aggressive subtypes of pancreatic cancer, with a median 5-year patient survival rate of <8% (1). Several studies have identified key molecular events that establish PDA. These efforts identified that genomic mutations activating KRAS are critical to disease manifestation in conjunction with inactivating tumor suppressors such as p53, SMAD4 or INK4A (2). Despite these efforts, actionable targets in PDA remain intractable. For example, developing effective KRAS inhibitors has been hampered due to its high affinity for GTP and a lack of deep pockets for the binding of small-molecule inhibitors (3). Several small-molecule compounds have been developed to inhibit the function of the KRAS proteins, exemplified by KRAS 'G12C' inhibitors; G12C mutations are rare in PDA (4).

Transcriptome profiling has identified molecular subtypes of PDA (5,6), which are likely coordinated by the cooperation of lineage-specific transcription programs. For example, lineage reprogramming of transcription factors (TFs) establishes the squamous subtype of PDA through activation of the squamous and suppression of the progenitor lineage programs, driven by activating a truncated isoform of p63 (ΔNp63) and ZBED2, respectively (7,8). Transcriptional changes also relate to the change of pathological states of PDA. Epithelial-to-mesenchymal transition (EMT), a process to gain migratory property during cancer progression, is a firmly established process regulated by EMT TFs (9). We previously demonstrated that FOXA1 activates the foregut developmental programs to drive PDA metastasis (10). FOXA2 was also found to be important in

*To whom correspondence should be addressed. Tel: +82 2 2123 2700; Fax: +82 2 362 9897; Email: jroe@yonsei.ac.kr
†The authors wish it to be known that, in their opinion, the first two authors should be regarded as Joint First Authors.

regulating unique gene expression programs in PDA cells, further enhancing the contribution of pancreatic developmental programs to tumorigenesis (11).

In this perspective, the central question in cancer research is how to discover a cancer-relevant gene expression program and its master regulators. Recent studies have identified super-enhancers (SEs) as a distinct type of *cis*-elements involved in cancer development (12,13). Characterized by extensive enrichment of histone modifications, such as acetylation of histone H3 lysine 27 (H3K27ac) and monomethylation of histone H3 lysine 4 (H3K4me1), and chromatin regulators (14), SEs potentially activate transcription programs involved in cancer malignancy (15,16). Recently, many studies have explored the biological activity of enhancer alteration in PDA (7,8,10,17–19). For example, SEs play an important role in determining the molecular subtype of PDA cells (19,20) and in modulating cellular crosstalk between PDA cells and tumor microenvironment (21). While SEs are associated with several driver genes in cancers, it remains elusive whether PDA cells deploy SE-driven oncogenic transcription programs via activating distinct downstream targets.

The ecotropic viral integration site 1 (EVI1) gene encodes a 145-kDa protein composed of 10 zinc fingers, and it is initially identified as an overexpressed gene resulting from retroviral insertion in mice or chromosomal rearrangements in human myeloid leukemia (22). EVI1 produces multiple splice variants generated via alternative splicing, and a major isoform is named EVI1Δ324, which lacks 324 amino acids including two zinc-finger (sixth and seventh) domains (23). Moreover, a small protein named MDS1 is produced nearby EVI1 locus. While EVI1 and MDS1 can be expressed separately, they can form an unusual but naturally occurring chimeric protein at transcriptional level, called MDS1/EVI1 (22). Functionally, EVI1 is a sequence-specific DNA binding protein and EVI1 downstream targets have been suggested to have potent oncogenic activity in leukemia (24). Ayoub *et al*. showed that conditional EVI1 overexpression in mice led to the leukemogenic transformation phenotype (25), which implicates that EVI1 may have oncogenic driver potential. Other than leukemia, analyzing clinical solid tumor samples showed frequent overexpression of EVI1 in colon, breast, ovarian and pancreatic cancers (26–29), but no recurrent chromosomal rearrangement involving the EVI1 locus in solid tumors has been reported so far. Detailed molecular mechanisms underlying EVI1 upregulation and its functional importance in PDA are yet to be determined. In this study, we identified that SE activates the cancer-specific EVI1 pathway and endows PDA pathogenesis. Our findings implicate selective inhibition of SE activity is a viable strategy to benefit the management of PDA.

## MATERIALS AND METHODS

### Cell culture conditions

Mouse pancreatic cancer cell lines KPC-2D and NB508 (kindly provided by Dr Nabeel Bardeesy) and the human pancreatic cancer cell line SUIT2 were cultured in Dulbecco's modified Eagle's medium (DMEM, Cat# LM001-05, WelGene) containing 10% (v/v) fetal bovine serum (FBS) (Cat# S001-01, WelGene) and antibiotics (Antibiotic-Antimycotic, Cat# 15240062, Gibco). HEK293T and Plat-E cells were maintained in DMEM with 5% FBS and antibiotics. Mouse pancreatic organoids were cultured as described previously (10). Briefly, organoids were plated with Matrigel (Cat# 356231, Corning) and mouse pancreas complete medium [advanced DMEM/F-12, 10 mM HEPES, Glutamax 1×, 500 nM A83-01, mEGF 50 ng/ml, mNoggin 100 ng/ml, hFGF10 100 ng/ml, 10 nM Gastrin I, 1.25 mM *N*-acetylcysteine, 10 mM nicotinamide, B-27 supplement (1× final), R-spondin 1 conditioned media (10% final)]. All the cells were grown at 37°C with 5% $CO_2$. All cell lines were regularly tested for mycoplasma with the PCR detection kit (REF# 25235, LiliF Diagnostics). For the Tet-ON system, doxycycline (Dox, 1 μM, CAS# 24390-14-5, Acros Organics) was treated at a fresh medium.

### Protein and DNA/RNA-related experiments

*Plasmid construction and shRNA cloning.* For the overexpression experiment, mouse EVI1 (Cat# 101858, Addgene) and human WNT7A (clone# hMU008519, KRIBB) cDNA constructs were purchased and subcloned into viral vectors (PiG, Addgene #18751; MSCV-neo, Addgene #105505; pCW57, Addgene #71782). For the knockdown experiment, short-hairpin RNAs (shRNAs) targeting EVI1 were cloned into the retroviral vector (LEPG, Addgene #111160; LT3GEPIR, Addgene #111177). TCF/LEF luciferase reporter vector, TOPFlash, was purchased from Addgene (#12456). All shRNA sequence (97-mer) information is listed in Supplementary Table S7.

*Virus production.* Retrovirus was prepared by plasmid DNA and packaging plasmids (VSVG and Eco-Helper) using OPTI-MEM (Cat# 31985070, Gibco) and polyethylenimine (PEI, Cat# 19850, Polysciences) in Plat-E cells. Lentivirus was prepared by plasmid DNA and packaging plasmids (VSVG and PAX2) using OPTI-MEM and PEI in HEK293T cells. Medium was replaced 6 h after transfection. Virus-containing supernatant was harvested for 3 days and filtered through 0.45-μm filters. Infection of pancreatic cancer cells was conducted with 0.5 ml filtered virus, 0.5 ml culture media and 20 μg/ml of polybrene (Cat# H2968, Sigma-Aldrich) in a 12-well plate. After 24 h of incubation, the culture medium was changed and selected with antibiotics (puromycin 1 μg/ml or G418 1 mg/ml). KPC-2D and NB508 stable and conditional cell lines were established by puromycin selection: PiG-empty, PiG-EVI1, PiG-EVI1-Flag, LEPG-shRen, LEPG-shEVI1, pCW57-empty, pCW57-EVI1, LT3GEPIR-shRen and LT3GEPIR-shEVI1. SUIT2 stable overexpression cell lines were established by G418 selection: MSCV-neo-empty and MSCV-neo-EVI1.

*Western blot.* Cultured cells were washed with 1 ml phosphate-buffered saline (PBS) and 1 million cells were counted. Cells were resuspended in 150 μl RIPA buffer [150 mM NaCl, 50 mM Tris–Cl (pH 8.0), 1% NP-40, 0.5% sodium deoxycholate, 0.1% sodium dodecyl sulfate (SDS) and protease inhibitor cocktail] and then incubated for 10

min at ice. These whole-cell lysates were centrifuged for 10 min at 4°C. The supernatant was mixed with 50 μl of 5× sample buffer [Bromophenol Blue 0.25%, DTT 0.5 M, glycerol 50%, SDS 10%, 0.25 M Tris–Cl (pH 6.8)]. The lysed sample was boiled at 95°C for 10 min. Each sample was loaded and separated by 9–10% SDS-PAGE gel electrophoresis and transferred onto nitrocellulose membranes at 4°C for 3 h. The membrane was blocked in 5% skimmed milk in Tris-buffered saline and Tween 20 (TBST) for 30 min. The blocked membrane was overnight incubated with the corresponding primary antibodies at 4°C. The membrane was washed with TBST and incubated with secondary antibodies for 40 min at room temperature. The membrane was washed with TBST and visualized using ECL solution (REF# 186309716, Thermo Scientific). The primary antibodies were VINCULIN (sc-73614, Santa Cruz), TUBULIN (sc-23948, Santa Cruz), EVI1 (2593S, Cell Signaling), WNT7A (10605-1-AP, Protein Tech) and BRD4 antibody (A301-985A50, Bethyl Laboratories).

*cDNA synthesis and RT-qPCR.* Total RNA was extracted using QIAzol reagent, and DNase I (Cat# AMPD1-1KT, Sigma-Aldrich) was used to prevent genomic DNA contamination. Purified RNA was quantified with the NanoDrop spectrophotometer. The 5× Prime Script Reverse Transcriptase (Cat# RR036A-1, Takara) and 2000 ng of RNA were used to synthesize complementary DNA. The expression was analyzed by qPCR by using SYBR Green Master Mix (REF# 4367659, Thermo Scientific). The relative expression was analyzed using a comparative cycle threshold method normalized with housekeeping gene, TBP. All quantitative reverse transcription PCR (RT-qPCR) primer information is listed in Supplementary Table S7.

### Dual-luciferase assay

A total of $1 \times 10^5$ KPC-2D cells were seeded in a six-well plate. The WNT reporter plasmid, TOP and Renilla plasmid were transfected into KPC-2D cells by using the jetPRIME method (REF# 712-60 and 114-15, Polyplus-transfection). The medium was replaced with a fresh medium (or conditioned medium) after 6 h. A dual-luciferase assay was performed after 72 h of transfection using the Promega dual luciferase kit (REF# E1910, Promega). The firefly luciferase level was normalized by Renilla activity.

### *In vitro* tumorigenesis assays

*Proliferation and anchorage-independent growth assay.* For a cell proliferation assay, $5 \times 10^4$ cells were resuspended in 2 ml growth medium and seeded in six-well plates. After 48 h of incubation, the number of cells in each well was quantified every day. For an anchorage-independent sphere formation assay, $1.5 \times 10^4$ cells were resuspended in serum-free DMEM with B-27 (final 1×, Cat# 17504044, Gibco) supplement and heparin (CAS# 9041-08-1, Sigma) and seeded in an ultralow attachment 24-well plate (REF# 3473, Corning). For the Tet-ON system, Dox was treated immediately after cells were seeded in a six-well plate or ultralow attachment plate, and replenished every 24 h. Images of cells were captured by a microscope on day 4 and the number of spheres was counted by using the ImageJ tool. All quantified data were plotted and analyzed by Prism application.

*Wound healing, ORIS and transwell cell migration assay.* For a wound healing migration assay, $1 \times 10^6$ cells per well in six-well plates were seeded and incubated for 24 h. When the cell confluence reached ∼90%, each well was scratched using a 200-μl pipette tip. To remove cell debris after scratching, cells were washed with PBS and replaced with a fresh medium. For the Tet-ON system, Dox was included in a fresh medium and replenished every 24 h. After indicated time at the figure, cells were treated with Syto13 reagent, and wound size was visualized by using microscopy. For the ORIS cell migration assay, the ORIS kit (Cat# CMAUFL4, Platypus Technologies) was used. A total of $2 \times 10^5$ cells were seeded at a provided 96-well plate. After the overnight incubation, the stopper was removed from the plate and a fresh medium was added. For the Tet-ON system, Dox was included in a fresh medium and replenished every 24 h. After indicated time at the figure, the cells were stained by Syto13 reagent and visualized by using microscopy. For the transwell migration assay, $1.5–4 \times 10^5$ cells in 250 μl serum-free medium were plated in the upper chamber. The upper chamber containing a 24-well plate was incubated for 10 min at standard conditions (37°C with 5% $CO_2$). Ten minutes later, a medium containing 10% FBS was placed into the bottom chamber. For the Tet-ON system, Dox was added to a medium containing 10% FBS. After indicated time at the figure, cells within the transwell membrane were fixed with 3.7% formaldehyde, permeabilized with 100% methanol and stained with crystal violet. All the migrated cells were visualized by using microscopy and counted by the ImageJ tool.

### *In vivo* tumorigenesis assay

The Yonsei IACUC approved all mouse experiment procedures. Five- to six-week-old male C57BL/6J mice were purchased from DBL and raised under semi-SPF conditions. For a mouse allograft, KPC-2D stable cells were subcutaneously injected in mice. A total of $0.5–1 \times 10^6$ cells were prepared in total volume 100 μl of PBS and 50 μl of Matrigel (REF# 356231, Corning). For Dox-induced EVI1/shEVI1 experiments, Dox chow (625 mg/kg, DooYeol Biotech) and Dox-containing water (2 mg/ml Dox with 5% sucrose, Sigma-Aldrich) were supplied. The length and width of tumors were regularly measured with a digital caliper. The tumor volume calculation followed the formula $0.5 \times \text{length} \times (\text{width})^2$. After ∼30 days of tumor cell implantation, all mice were sacrificed, and the tumor allografts were excised.

### Statistics

All statistical analyses were performed in Prism (GraphPad Software) and presented as mean ± standard error of mean (SEM). An unpaired *t*-test was employed to evaluate significance by using a $P$-value $<0.05$.

## RESULTS

### SE drives aberrant EVI1 expression in advanced PDA cells

We previously demonstrated that reprogrammed enhancer landscape is crucial for PDA progression (10). That study generated genome-wide H3K27ac enrichment profiles in $Kras^{+/LSL\text{-}G12D}$, $Trp53^{+/LSL\text{-}R172H}$, and Pdx1-Cre from normal pancreatic duct ($N^5$, $N^6$), pancreatic intraepithelial neoplasia ($P^2$, $P^3$), primary tumor ($T^3$, $T^6$, $T^{19}$, $T^{23}$, $T^{33}$, $T^{34}$) and metastasis ($M^{1L}$, $M^{3L}$, $M^{3P}$, $M^{6P}$, $M^{10P}$, $M^{15D}$). We hypothesized that characterization of H3K27ac SEs could identify core regulatory factors in PDA. By implementing the rank ordering of super-enhancer (ROSE) algorithm (12,30), we identified a total of 2345 H3K27ac SEs across these 16 organoids (Supplementary Table S1). Based on the prior observation that M organoids possess massively altered H3K27ac enhancer activity linked to PDA biology, we sought to identify H3K27ac SE constituents specifically activated in M organoids. When we determined the value of M-specific H3K27ac SE activity at 2345 SEs, represented from $\log_2$ fold change (fc) of averaged H3K27ac signal of six M organoids divided by two N organoids, we noticed that five EVI1-associated distal enhancers (e1–e5) ranked at the top (Figure 1A; Supplementary Figure S1A). We further confirmed that EVI1 H3K27ac SE domains are activated exclusively and recurrently in M organoids, except diaphragm-derived $M^{15D}$, with the genome browser track, although the degrees vary (Figure 1B; Supplementary Figure S1B). From RNA sequencing (RNA-seq), RT-qPCR and western blotting, we found that increased EVI1 expression correlates with M-specific H3K27ac SE activity (Figure 1C and D; Supplementary Figure S1C). Although we have primarily focused on EVI1, several SEs are located near genes known to have PDA-relevant biology, including roundabout guidance receptor 1 (ROBO1), semaphorin 7A (SEMA7A), glycine decarboxylase (GLDC) and sterol *O*-acyltransferase 1 (SOAT1) (data not shown). ROBO1 and SEMA7A, regulators of axon guidance, are implicated in pancreatic carcinogenesis (31). GLDC and SOAT1 are involved in the hypermetabolic growth of PDA cells by regulating the serine–glycine–one-carbon pathway and the mevalonate pathway, respectively (32,33).

Next, we interrogated publicly available transcriptome data of human cancer cell lines (34). We observed pervasive EVI1 expression in most human PDA cell lines, whereas non-neoplastic pancreatic cell lines barely express EVI1 (Supplementary Figure S1D). Analysis of the curated TCGA (The Cancer Genome Atlas) PDA dataset excluding samples of normal pancreas or low cellularity tumors (2,35) showed no significant association between EVI1 overexpression and inferior prognosis of PDA patients (Supplementary Figure S1E). This analysis indicates that EVI1-low tumors can achieve poor patient outcomes through EVI1-independent mechanisms. Nevertheless, we found gradually increased EVI1 expression during PDA progression (Supplementary Figure S1F). Dense stromal and immune compartments within tumors cause extremely heterogeneous pathological features of PDA (36). By re-analyzing single-cell RNA-seq (scRNA-seq) data of 11 human normal pancreatic tissues and 24 human PDA (37), we concluded that an epithelial compartment of cancer tissue is an origin of massive EVI1 expression (Figure 1E and F; Supplementary Figure S1G). Our findings indicate that EVI1 expression and PDA progression are interrelated.

We next reasoned that identifying TFs that bind to EVI1 SEs would identify potential mediators of EVI1 upregulation. We focused on five EVI1 SE domains to find TF motif enrichment using the TRAP motif discovery algorithm (38). To this end, we found a total of 14 TF motifs that are significantly enriched at EVI1 SEs (Supplementary Figure S1H). The list of enriched motifs includes DNA binding sites for the Forkhead and the GATA families of TFs. We have previously shown that elevated expression of FOXA1 and GATA5 is associated with PDA progression and enhancer activation (10). Including FOXA1 and GATA5, TF motif analyses at EVI1 SEs identified an association with motifs recognized by FOXF2, RUNX3, PAX9, FOSL1 and GATA3, which are transcriptionally upregulated TFs in M organoids (Supplementary Figure S1I). Using the published dataset, we confirmed that EVI1 SEs are occupied by FOXA1 in M organoids (Supplementary Figure S1J), although FOXA1 overexpression alone is not sufficient to transactivate EVI1 (10). Nevertheless, our analyses implicate core TFs that are critical for establishing EVI1 SEs.

We then determined whether H3K27ac SE activation had a causal role in EVI1 upregulation. Small-molecule SE inhibitors were available; we therefore tested whether EVI1 expression is sensitive to perturbing SE activity pharmacologically. Experimentally, we decided to displace bromodomain-containing protein 4 (BRD4), a known component of SE, from chromatin with JQ1 (39). By conducting a genome-wide chromatin immunoprecipitation sequencing (ChIP-seq) assay, we found that BRD4 selectively binds to SE in M organoid (Figure 1G). To examine whether SE-mediated EVI1 upregulation is conserved phenomenon, we chose paired $T19/M^{6P}$ and $T6/M^{3P}$ organoids established from the same source. RT-qPCR and western blotting analyses revealed that inhibiting SE activity with JQ1 (1 μM for 48 h) in M organoids resulted in marked EVI1 reduction in both mRNA and protein levels in paired T–M organoids (Figure 1H and I). Our findings collectively suggest the epigenetic basis of aberrant EVI1 expression and its clinical relevance to the PDA.

### EVI1 overexpression directs transcriptional remodeling and aggressive phenotypes in PDA cells

Our preliminary epigenomic and transcriptomic analyses implicate a pro-tumorigenic activity of EVI1 in PDA cells. Thus, we conducted gain-of-function experiments to examine the biological importance of EVI1 upregulation. To perform *in vitro* assays of pro-tumorigenic potential, we used monolayer culture, the KPC-2D cells, established previously (10). While the KPC-2D cells are a cell line derived from a T organoid, it lacks the wild-type Trp53 allele and had allowed to perform *in vitro* assays of pro-tumorigenic phenotypes (10). We also chose KPC-2D cells for both gain- and loss-of-function experiments by considering its modest EVI1 mRNA expression (10). Once the KPC-2D cells were retrovirally transduced with mouse EVI1 cDNA, we con-

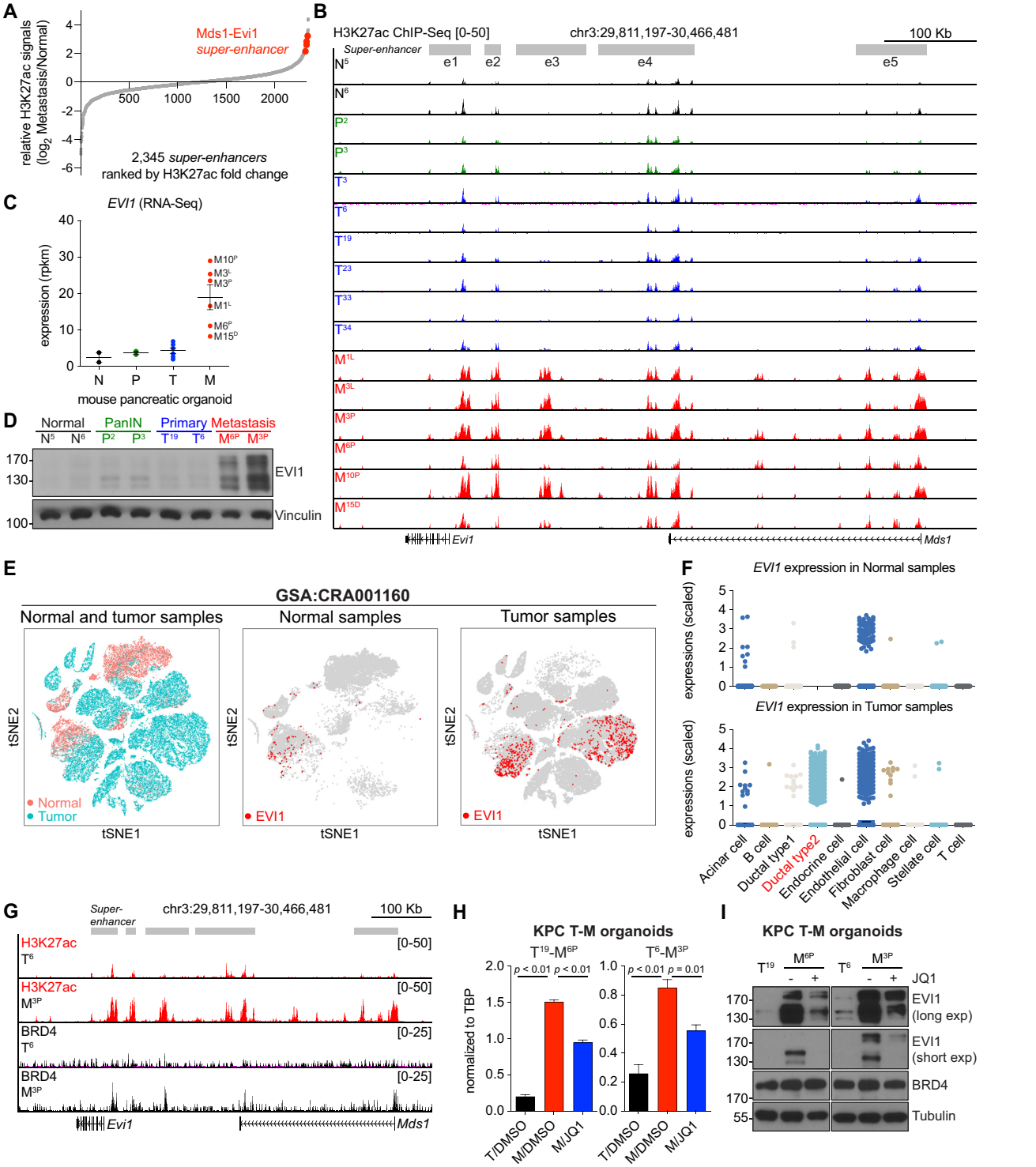


**Figure 1.** SE drives the aberrant EVI1 expression in advanced PDA cells. (**A**) Ranking of relative H3K27ac signals in mouse pancreatic metastasis organoids to normal organoids. A total of 2345 SEs were identified using the ROSE algorithm. (**B**) ChIP-seq profiles of H3K27ac in mouse normal ($N^5$, $N^6$), PanIN (pancreatic intraepithelial neoplasia; $P^2$, $P^3$), primary tumor ($T^3$, $T^6$, $T^{19}$, $T^{23}$, $T^{33}$, $T^{34}$) and metastasis ($M^{1L}$, $M^{3L}$, $M^{3P}$, $M^{6P}$, $M^{10P}$, $M^{15D}$) organoids at the MDS and EVI1 loci. $M^{1L}$ and $M^{3L}$ are liver metastasis-derived organoids. $M^{3P}$, $M^{6P}$ and $M^{10P}$ are peritoneal metastasis-derived organoids. $M^{15D}$ is diaphragm metastasis-derived organoid. Predicted SEs are shown in gray above the genome browser tracks. (**C**) EVI1 mRNA expression in mouse organoids. Mean ± SEM is shown. (**D**) Western blot analysis for EVI1 in the indicated organoids. (**E**) scRNA-seq analysis from 11 normal pancreatic tissues and 24 human PDA tumor samples. (**F**) EVI1 expression across cell types shown in normal (top) and tumor samples (bottom). (**G**) ChIP-seq profiles of BRD4 in the indicated organoids at the MDS and EVI1 loci. (**H**) RT-qPCR for EVI1 expression in $T^{19}$/DMSO or $M^{6P}$ (DMSO or JQ1), and $T^6$/DMSO or $M^{3P}$ (DMSO or JQ1). The indicated organoids were treated with DMSO or 1 μM JQ1 for 48 h. Mean ± SEM is shown, and *P*-value was determined by Student's *t*-test. (**I**) Western blot analysis for EVI1 expression in $T^{19}$/DMSO or $M^{6P}$ (DMSO or JQ1), and $T^6$/DMSO or $M^{3P}$ (DMSO or JQ1). See also Supplementary Figure S1.

firmed EVI1 overexpression with a western blotting experiment (Figure 2A). EVI1 overexpression enhanced proliferation, anchorage-independent growth and migration (Figure 2B and C; Supplementary Figure S2A–G). These phenotypes are not restricted to a murine PDA cell line, as we observed similar results in a human PDA cell line, SUIT2, overexpressing above EVI1 cDNA construct (Supplementary Figure S2H–J). More importantly, when we transplanted EVI1-overexpressing or control cells into the syngeneic mice, we found substantially increased growth rate and the size of subcutaneous tumors by EVI1 overexpression (Figure 2D and E). These findings strongly suggest that EVI1 upregulation endows the acquisition of aggressive behaviors in PDA cells.

Although EVI1 protein is composed of multiple zinc-finger domains, it remains unclear how EVI1 controls specific gene expression programs in cancer cells. Our prior work showed that FOXA1-driven altered enhancer activity is responsible for PDA metastasis (10). It is possible that selective enhancer reprogramming similarly explains EVI1-driven tumorigenesis. To test our hypothesis, we performed ChIP-seq experiments with antibodies recognizing H3K27ac and H3K4me1. We also measured chromatin accessibility via assay for transposase-accessible chromatin with sequencing (ATAC-seq) experiments (40). With interest in EVI1-activated enhancer elements, we prioritized to isolate regions where H3K27ac are enriched >4-fold upon EVI1 overexpression than control. As a result, we recovered 496 sites having elevated H3K27ac signal from a total of 65 703 H3K27ac-occupied sites, hereafter referred to as 'EVI1-*GAIN* regions' (Figure 2F; Supplementary Table S2). Like previously reported FOXA1-*GAIN* regions, non-promoter regions consist of 88.5% of EVI1-*GAIN* regions (Figure 2F). A meta-analysis from the EVI1-*GAIN* regions also revealed increased H3K4me1 enrichment and chromatin accessibility in EVI1-expressing cells (Figure 2G). We also found that the Flag-EVI1 ChIP-seq signal concentrates at these sites. Our findings suggest that EVI1 overexpression promotes activation of 496 *GAIN* enhancer regions. However, only ∼1% of these EVI1-*GAIN* regions (5/496 regions) overlapped with FOXA1-*GAIN* regions (Supplementary Figure S2K); EVI1 and FOXA1 are therefore not functionally redundant.

To associate EVI1-*GAIN* enhancer regions with putative EVI1 target genes, we identified 445 unique enhancer proximal genes (hereafter referred to as 'EVI1-*GAIN* genes'), 51 genes associated with >1 enhancer peak. Based on the gene set enrichment analysis (GSEA) of RNA-seq data obtained from EVI1-expressing or control cells, we found that expression changes of EVI1-*GAIN* genes significantly correlated with enhancer activity in mouse and human PDA cells (Figure 2H; Supplementary Figure S2L; Supplementary Tables S3 and S4). Gene Ontology (GO) analysis of EVI-*GAIN* genes with the Gene Ontology Consortium tool (41,42) revealed associations of these genes with pro-tumorigenic signatures (Figure 2I; Supplementary Table S5). For example, the heatmap representation of genes in 'regulation of cell motility', including the EVI1-activated WNT7A gene, may explain EVI1-mediated increase of motility (Figure 2J; Supplementary Figure S2M and N). We also found associations with 'cellular component of biogenesis', 'response to decreased oxygen levels' and 'regulation of signal transduction' indicating that EVI1 activation can provide adaptation to low oxygen and nutrient levels during tumor development. To evaluate the cancer-relevant expression of EVI1-*GAIN* genes, we performed GSEA of PDA patient microarray data. Microarray gene expression profiles of paired pancreatic tumor and non-tumor tissues from three independent studies revealed increased expression of EVI1-*GAIN* genes in tumor compared to non-tumor samples (Figure 2K). These findings implicate the tight association between EVI1-driven enhancer reprogramming and tumor aggressiveness in PDA cells.

### Inducible EVI1 overexpression identifies a sequential activation process of EVI1-*GAIN* enhancers

Chromatin accessibility precedes establishing a unique histone modification pattern by enhancer activation on adjacent nucleosomes (43,44). Among variable histone modifications, H3K4me1 is exclusively presented at enhancers regardless of whether they are active or not, whereas H3K27ac is presented specifically at potentially active enhancers, not at inactive enhancers/promoters (45). Based on this, we decided to examine a sequential process of enhancer activation by EVI1 overexpression. To establish a system suitable for monitoring sequential chromatin changes, we established KPC-2D cells expressing EVI1 in a Dox-dependent manner using a lentivirus-based tetracycline-inducible (Tet-ON) system. After we confirmed that Dox induced EVI1 expression by 24 h and maintained the expression for at least 96 h (Supplementary Figure S3A), we conducted ATAC-seq, ChIP-seq (H3K4me1 and H3K27ac) and RNA-seq experiments. From a meta-analysis of EVI1-*GAIN* regions, we found that a brief induction of EVI1 protein resulted in an immediate increase of chromatin accessibility, followed by sequential changes of H3K4me1 and H3K27ac (Figure 3A and B; Supplementary Figure S3B). We presumed that signals at EVI1-*GAIN* regions reached maximum at 72 h upon Dox treatment. Based on this criterion, chromatin accessibility increased by >90% in KPC-2D cells at 24 h of EVI1 induction, whereas the increase of H3K4me1 and H3K27ac enrichment by 90% requires 48 and 72 h, respectively (Figure 3C). More importantly, GSEA of RNA-seq datasets revealed a gradually increasing pattern of GSEA enrichment scores from 24 to 72 h, as exemplified by the WNT7A gene (Figure 3D; Supplementary Figure S3C). These data support the importance of EVI1-mediated coordination for chromatin accessibility and enhancer activity. Phenotypically, consistent with the stable EVI1 expression setting, induction of EVI1 expression led to pro-tumorigenic phenotypes *in vitro* (Figure 3E and F; Supplementary Figure S3D–I). In contrast to the stable expression of EVI1, Dox-inducible EVI1 expression showed marginal effect on the increased cell proliferation *in vitro* (Supplementary Figure S3J), while it increased subcutaneous tumor growth *in vivo* (Figure 3G–I). These findings suggest that EVI1 modulates transcriptional enhancer remodeling associated with tumorigenesis.

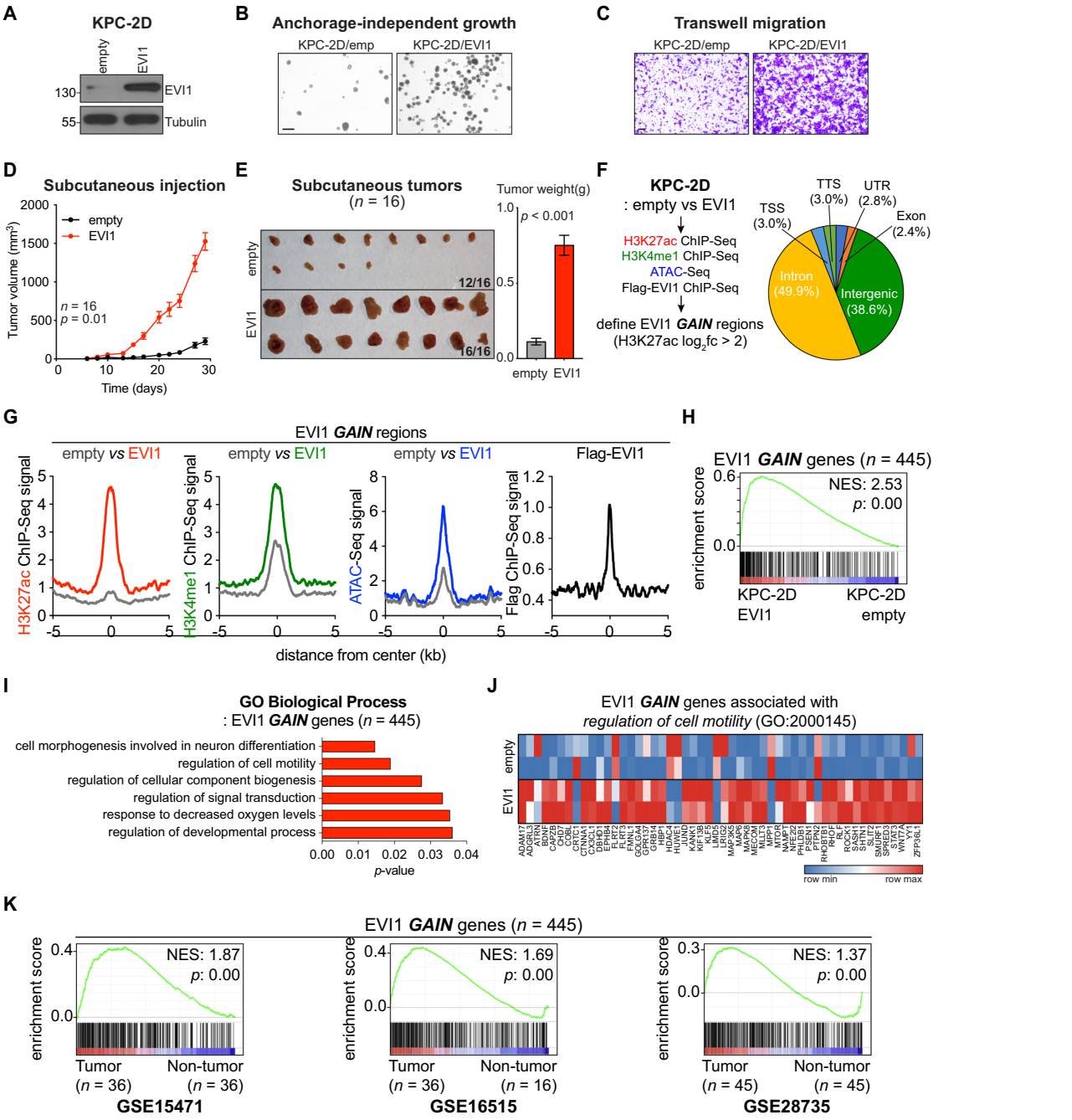


**Figure 2.** EVI1 drives aggressive phenotypes and transcriptional remodeling in PDA cells. (**A**) Western blot analysis for EVI1 in whole-cell lysates prepared from KPC-2D cells stably expressing EVI1 cDNA (KPC-2D/EVI1) or control (KPC-2D/empty). (**B**) Anchorage-independent growth of KPC-2D/empty and KPC-2D/EVI1 cells. Bright-field images were taken at 96 h after cell seeding. Scale bars: 100 μm. (**C**) Transwell migration assay of KPC-2D/empty and KPC-2D/EVI1 cells. The migrated cells were stained with crystal violet at 24 h after seeding and bright-field images were taken. Scale bars: 100 μm. (**D**) Graph shows subcutaneous tumor growth after injection of KPC-2D/empty and KPC-2D/EVI1 ($5 \times 10^5$ cells per each injection, $n = 16$) cells in C57BL/6J mice. Tumor volumes were measured every 2 days after injection for 30 days. (**E**) Bright-field images of tumors removed from mice (left) and quantification of tumor weights (right) 30 days after injection of KPC-2D/empty and KPC-2D/EVI1 in C57BL/6J mice. Means ± SEMs are shown. (**F**) Schematic diagram demonstrating analysis used to determine the function of EVI1 on chromatin (left) and pie chart showing the genomic annotations of 496 EVI1-*GAIN* regions according to the location of a given peak (right). TSS, '−1 kb to +100 bp' of transcription start sites; TTS, '−100 bp to +1 kb' of transcription termination sites. UTR includes both 5′ and 3′ untranslated regions. (**G**) Metagene representation of the ChIP-seq signal for the indicated histone marks, the ATAC-seq signal and Flag-EVI1 ChIP-seq signal across EVI1-*GAIN* regions in KPC-2D/empty or KPC-2D/EVI1 cells. Metagenes are centered on the middle of *GAIN* regions and 10 kb around the center of *GAIN* regions are displayed. (**H**) GSEA of KPC-2D/empty versus KPC-2D/EVI1 RNA-seq using a signature of EVI1-*GAIN* genes. Normalized enrichment score (NES) and nominal *P*-value were provided according to GSEA. (**I**) GO analysis of genes located nearest to EVI1-*GAIN* regions. Only significantly enriched GO terms related to biological process are shown. (**J**) Heatmap representation of EVI1-*GAIN* genes associated with regulation of cell motility in KPC-2D/empty and KPC-2D/EVI1 cells. (**K**) GSEA of pancreatic tumor versus non-tumor microarray using a signature of EVI1-*GAIN* genes. Publicly available PDA patient data (GSE15471, GSE16515 and GSE28735) were used for the analysis. NES and nominal *P*-value were provided according to GSEA. See also Supplementary Figure S2.

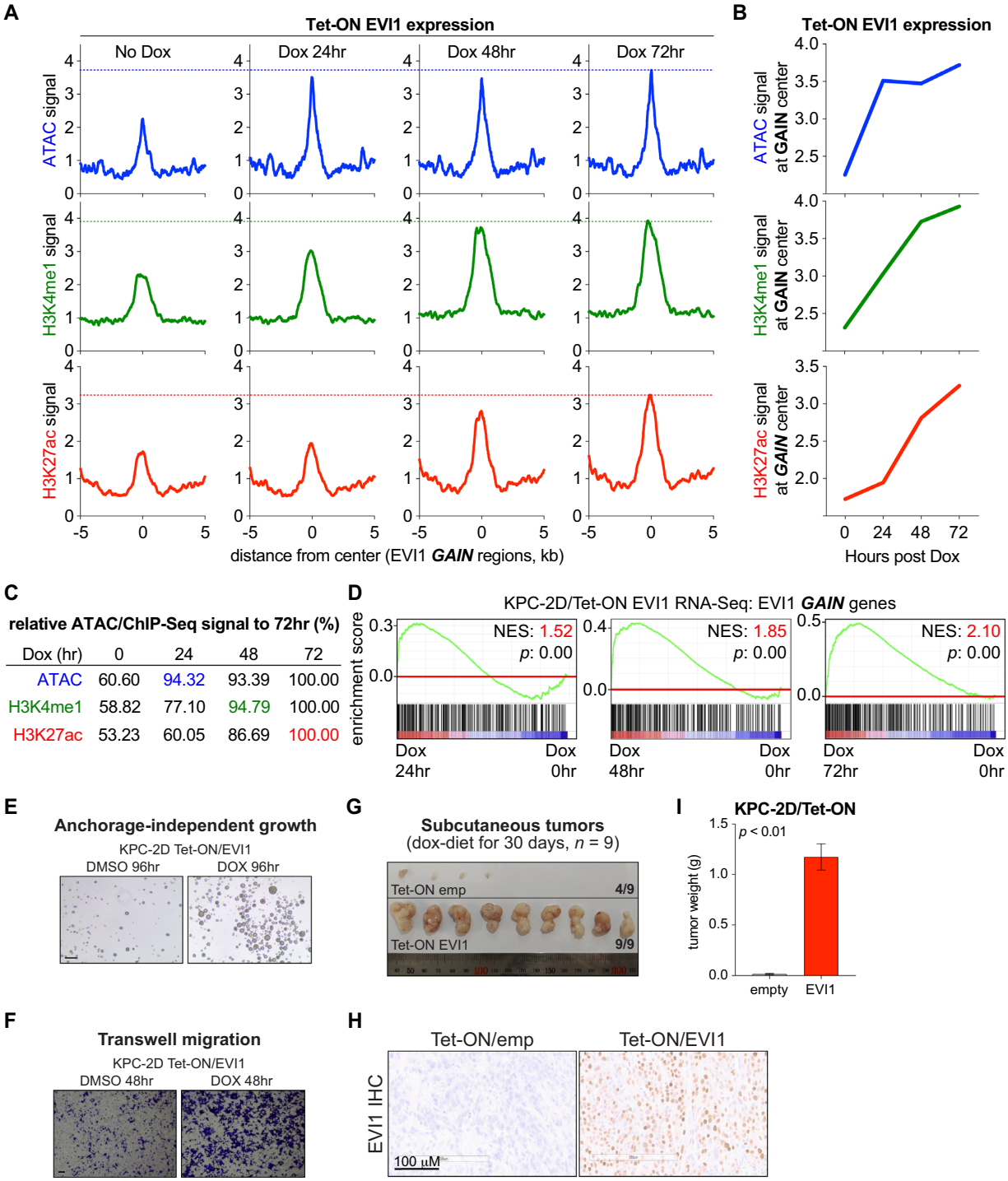


**Figure 3.** Inducible EVI1 expression identifies activating process of EVI1-*GAIN* enhancers. (**A**) Metagene representation of the ATAC-seq and ChIP-seq signals for H3K4me1 and H3K27ac across EVI1-*GAIN* regions in KPC-2D Tet-ON/EVI1 cells treated with 1 μM Dox for indicated periods of time. Metagenes are centered on the middle of EVI1-*GAIN* regions and 10 kb around the center of *GAIN* regions are displayed. (**B**) Graphs showing ATAC-seq and ChIP-seq signals for H3K4me1 and H3K27ac at the peak center in the KPC-2D Tet-ON/EVI1 cells treated with Dox from 0 to 72 h. (**C**) Quantification of results in (B), relative to signals at 72 h. (**D**) GSEA of RNA-seq using a signature of EVI1-*GAIN* genes of KPC-2D Tet-ON/EVI1 cells treated with Dox for 24, 48 or 72 h versus 0 h. NES and nominal *P*-value were provided according to GSEA. (**E**) Bright-field images of anchorage-independent growth of KPC-2D Tet-ON/EVI1 cells treated with DMSO or Dox for 96 h. Scale bars: 100 μm. (**F**) Transwell migration assay of KPC-2D Tet-ON/EVI1 cells treated with DMSO or Dox for 48 h. The migrated cells were stained with crystal violet, and bright-field images were taken. Scale bars: 100 μm. (**G**) Images of tumors developed for 30 days in C57BL/6J mice after subcutaneous injection of $1 \times 10^6$ KPC-2D Tet-ON/empty or KPC-2D Tet-ON/EVI1 cells and receiving Dox-supplemented diet. Note that four mice transplanted with KPC-2D Tet-ON/empty cells did not show apparent tumor formation. (**H**) Representative immunohistochemical staining for EVI1 of tumor samples from (G). Scale bars: 100 μm. (**I**) Bar graph showing subcutaneous tumor weight 30 days after injecting $1 \times 10^6$ KPC-2D Tet-ON/empty or KPC-2D Tet-ON/EVI1 cells in C57BL/6J mice ($n = 9$ for each cell strain). See also Supplementary Figure S3.

### EVI1 depletion impairs tumor-intrinsic programs and PDA tumorigenesis

To examine whether the aggressive phenotype of PDA cells depends on EVI1, we generated EVI1-deficient KPC-2D cells with shRNAs. We conducted western blotting to examine the EVI1 protein level in KPC-2D cells stably expressing a control shRNA or different EVI1 shRNAs and found #2 as the most potent shRNA in reducing EVI1 (Supplementary Figure S4A). Further RT-qPCR and western blotting analyses validated that EVI1 protein expression is suppressed >2-fold in cells expressing #2 shRNA (Figure 4A). We used these cultures to characterize phenotypes affected by EVI1 depletion. EVI1-depleted cells proliferated slower and had reduced anchorage-independent growth and migration than control cells *in vitro* (Figure 4B and C; Supplementary Figure S4B–D). When injected subcutaneously into syngeneic mice, EVI1-depleted cells formed smaller tumors than control cells (Figure 4D). Our loss-of-function investigation suggested that EVI1 expression is important for the aggressiveness of PDA cells *in vitro* and *in vivo*.

The above findings led us to investigate whether EVI1 expression is critical to keep aberrant gene expression programs. GSEA of RNA-seq data from EVI1-depleted and control cells verified significant downregulation of EVI1-*GAIN* gene enrichment in EVI1-depleted cells (Figure 4E; Supplementary Table S6). We use another mouse pancreatic cancer cell line, NB508, derived independently from the KPC mouse to confirm the results from KPC-2D cells. Following the generation of NB508 cells expressing EVI1 shRNA #2 or control shRNA, we conducted RNA-seq analysis. Consistent with the observation from KPC-2D cells, EVI1 depletion led to significant suppression of EVI1-*GAIN* gene enrichment in NB508 cells (Supplementary Figure S4E; Supplementary Table S6). Similar to KPC-2D cells, EVI1 depletion impairs anchorage-independent growth and migration than control in NB508 cells (Supplementary Figure S4F–I).

To define the EVI1 pathway in PDA cells, we analyzed the RNA-seq dataset from KPC-2D cells expressing EVI1 cDNA and that from KPC-2D cells expressing EVI1 shRNA. We defined EVI1's target genes as those whose expression changes at opposite directions with EVI1 overexpression and EVI1 knockdown. As a result, we identified a total of 79 genes that were increased with EVI1 overexpression and decreased with EVI1 knockdown (Figure 4F). The GO annotations associated with EVI1-*GAIN* genes were similarly enriched for these 79 genes (Figure 4G), indicating that these genes represent transcriptional outputs of reprogrammed enhancers. In the NB508 cell line, top downregulated genes upon EVI1 knockdown were enriched for similar GO terms as in KPC-2D cells, including 'positive regulation of cell migration' (Supplementary Figure S4J and K). In agreement with EVI1 cDNA overexpression experiments, EVI1 knockdown reduces EVI1-*GAIN* enhancer activity, exemplified by the WNT7A locus (Supplementary Figure S4L).

Prompted by the above findings, we generated KPC-2D cell lines expressing EVI1 shRNA in a Dox-inducible manner. The western blotting experiment confirmed the downregulation of EVI1 protein expression upon Dox treatment (Figure 4H). Consistent with the results from a stable knockdown, Dox-induced EVI1 depletion resulted in reduced anchorage-independent growth and less migratory ability *in vitro* (Figure 4I and J; Supplementary Figure S4M and N). Mechanistically, Dox-dependent suppression of EVI1-*GAIN* gene expression explains these phenotypes, exemplified by the WNT7A gene (Figure 4K; Supplementary Figure S4O and P; Supplementary Table S6). To examine whether induced EVI1 knockdown influences tumor growth *in vivo*, KPC-2D cells expressing conditional shEVI1 or control shRNA were injected subcutaneously and maintained on the Dox diet for 4 weeks. As a result, we found that EVI1 knockdown reduced subcutaneous tumor size and volume significantly, suggesting that tumor growth depends on sustained EVI1 expression (Figure 4L and M). Our above findings indicate that EVI1 is important for the growth of PDA tumors.

### EVI1–WNT7A is a key axis of EVI1-driven transcription changes and PDA aggressiveness

Since our data establish that EVI1 is important for aggressive PDA cells, we were prompted to identify potentially druggable targets of the EVI1 pathway. To nominate primary EVI1 downstream targets, we utilized conditional EVI1 expression or knockdown systems described above. We harvested RNA from cells induced to overexpress or deplete EVI1 for 24 h and subjected them for RNA-seq. We defined prominent target genes of EVI1 transactivation as those whose expression rapidly increased or decreased upon EVI1 induction or depletion, respectively. To this end, we found the WNT7A gene. WNT7A is among the top-upregulated and top-downregulated genes upon induction of EVI1 overexpression and knockdown, respectively (Figure 5A). The western blotting experiment validated RNA-seq analysis (Figure 5B). It is noteworthy that our bioinformatic analyses already nominated WNT7A as an example of enhancer reprogramming earlier in the study. WNT7A may also have a pro-tumorigenic function as it is functionally associated with GO annotations of cell migration.

We further examine whether WNT7A upregulation is clinically relevant and is associated with EVI1 expression. We compared EVI1 expression in normal tissues from the genotype-tissue expression datasets (46) or tumors from the TCGA Pan-Cancer Atlas and found that pancreatic cancer expressed the second highest level of WNT7A among examined human cancers, while WNT7A expression is barely detectible in the normal pancreas (Supplementary Figure S5A and B). Analyzing publicly available single-cell transcriptome data of PDA from patients further supports the cancer-specific expression pattern of WNT7A, similar to EVI1 (Figure 5C). Notably, both EVI1 and WNT7A are selectively expressed in the same tumor-derived ductal compartment, ductal type 2 (Supplementary Figure S1F; Figure 5C), implicating that EVI1 and WNT7A upregulation is spatially associated. Subsequent transcriptome analysis of mouse PDA organoids validated a significant association between EVI1 and WNT7A mRNA levels (Figure 5D). Clinically, we observed a gradually increased WNT7A mRNA expression pattern during pancreatic cancer progression (Figure 5E). Furthermore, TCGA pancreatic can-

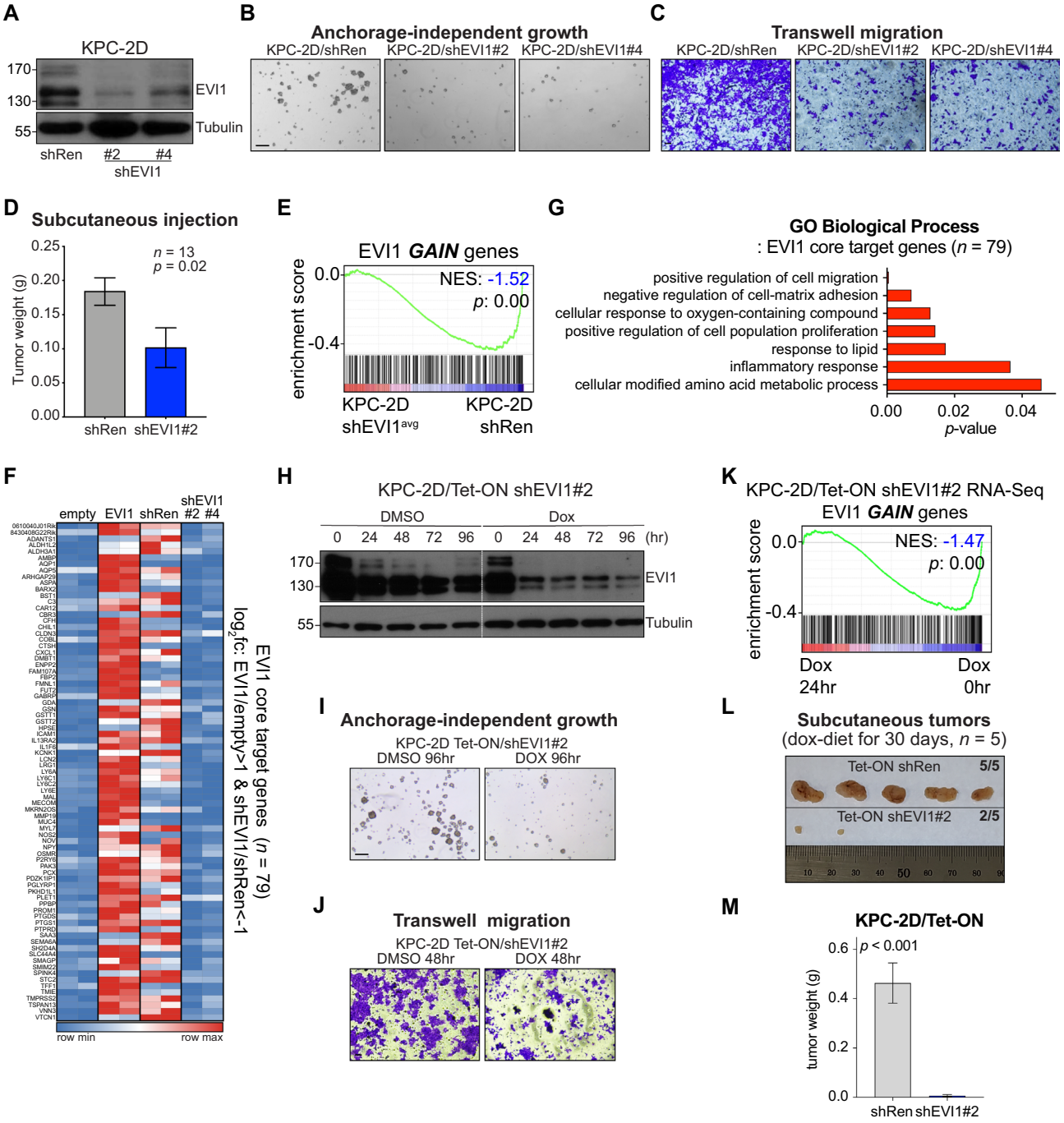


**Figure 4.** EVI1 depletion impairs PDA tumorigenesis with a defect in tumor-promoting programs. (**A**) RT-qPCR and western blotting for EVI1 expression in KPC-2D cells stably expressing shRen (KPC-2D/shRen) or shEVI1 #2 and #4 constructs (KPC-2D/shEVI1#2 and KPC-2D/shEVI1#4). (**B**) Bright-field images of anchorage-independent growth of KPC-2D/shRen and KPC-2D/shEVI1 cells at 96 h after seeding. Scale bars: 100 μm. (**C**) Transwell migration assay of KPC-2D/shRen and KPC-2D/shEVI1 cells. The migrated cells were stained with crystal violet at 24 h, and bright-field images were taken. Scale bars: 100 μm. (**D**) Bar graph showing subcutaneous tumor weight 30 days after injection of $1 \times 10^6$ KPC-2D/shRen or KPC-2D/shEVI1 cells in C57BL/6J mice ($n = 13$ in each group). (**E**) GSEA of KPC-2D/shEVI1 versus KPC-2D/shRen RNA-seq using a signature of *GAIN* genes. NES and nominal *P*-value were provided according to GSEA. (**F**) Heatmap representation of EVI1 core target genes in KPC-2D/empty, KPC-2D/EVI1, KPC-2D/shRen and KPC-2D/shEVI1 cells. EVI1 core target genes ($n = 79$) are defined as $\log_2$ fc $> 1$ in KPC-2D/EVI relative to KPC-2D/empty, and $\log_2$ fc $< -1$ in KPC-2D/shEVI1 relative to KPC-2D/shRen. (**G**) Ontology analysis of EVI1 core target genes. GO terms related to the biological process are shown. (**H**) Western blot analysis for EVI1 expression in KPC-2D Tet-ON/shEVI1 cells or KPC-2D Tet-ON/shRen. The cells were incubated with 1 μM Dox for 0, 24, 48, 72 and 96 h. (**I**) Bright-field images of anchorage-independent growth of KPC-2D Tet-ON/shEVI1 cells treated with DMSO or Dox for 96 h. Scale bars: 100 μm. (**J**) Transwell migration assay of KPC-2D Tet-ON/shEVI1 cells treated with DMSO or Dox for 48 h. The migrated cells were stained with crystal violet, and bright-field images were taken. Scale bars: 100 μm. (**K**) GSEA of RNA-seq in KPC-2D Tet-ON/shEVI1 treated with Dox for 24 h versus 0 h using a signature of EVI1-*GAIN* genes. NES and nominal *P*-value were provided according to GSEA. (**L**) The image of tumors harvested 30 days after C57BL/6J mice were subcutaneously injected with $1 \times 10^6$ KPC-2D Tet-ON/shRen or KPC-2D Tet-ON/shEVI1 cells and received Dox-supplemented diet ($n = 5$ in each group). Note that three mice transplanted with KPC-2D Tet-ON/shRen cells did not develop apparent tumor. (**M**) Quantification of tumor weight of tumors in (L). See also Supplementary Figure S4.

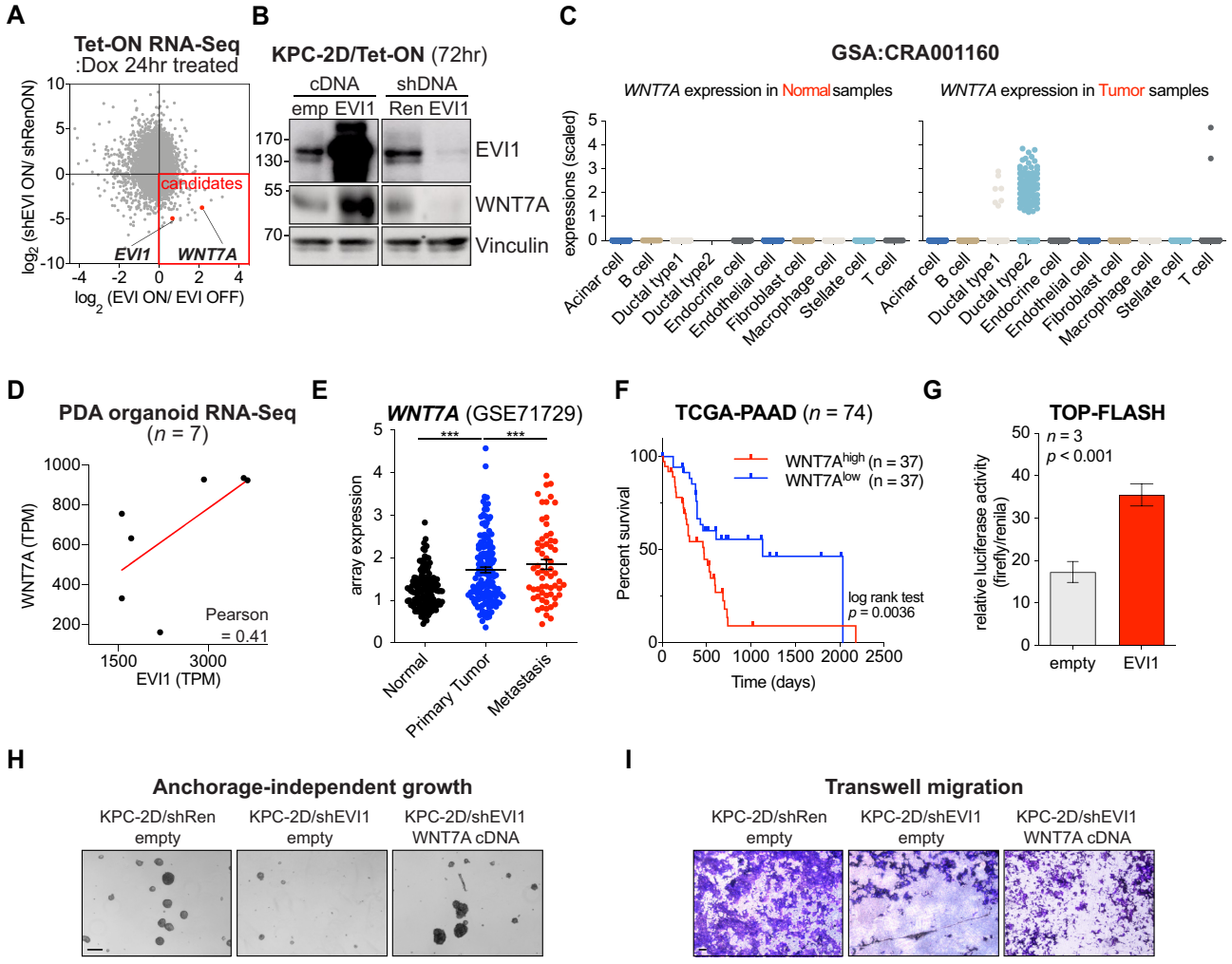


**Figure 5.** WNT7A is a critical target of EVI1-driven transcription changes and PDA aggressiveness. (**A**) Scatter plot comparing the expression of each gene (in $\log_2$ scale) in the Tet-ON EVI1/empty RNA-seq (*X*-axis) versus the Tet-ON shEVI1/shRen RNA-seq (*Y*-axis). KPC-2D Tet-ON/empty or EVI1, and KPC-2D Tet-ON/shRen or shEVI1 cells were treated with Dox for 24 h. (**B**) Western blot analysis for EVI1 and WNT7A proteins in KPC-2D Tet-ON/empty or EVI1 cells and in KPC-2D Tet-ON/shRen or shEVI1 cells incubated with Dox for 72 h. (**C**) scRNA-seq-based WNT7A expression analysis across cell types shown in normal (left) and tumor (right) samples. (**D**) Correlation between EVI1 and WNT7A transcript levels in PDA organoid RNA-seq. (**E**) Microarray-based WNT7A expression in normal pancreas and primary and metastatic PDA tumor samples. Mean ± SEM is shown. *P*-values were determined by Student's *t*-test. (**F**) Survival curves of patients stratified according to high or low expression of WNT7A in their PDA. Curated TCGA PDA patient samples ($n = 74$) were classified into two groups based on the mean expression value of WNT7A. *P*-value was calculated using the log-rank (Mantel–Cox) test. (**G**) Bar graph showing TOPFlash reporter expression in KPC-2D/empty or EVI1 cells. (**H**) Bright-field images of anchorage-independent growth of KPC-2D/shRen/empty, KPC-2D/shEVI1/empty and KPC-2D/shEVI1/WNT7A cells at 96 h after seeding. Scale bars: 100 μm. (**I**) Transwell migration assay of KPC-2D/shRen/empty, KPC-2D/shEVI1/empty and KPC-2D/shEVI1/WNT7A cells. The migrated cells were stained with crystal violet at 48 h, and bright-field images were taken. Scale bars: 100 μm. See also Supplementary Figure S5.

cer patients whose tumor highly expresses WNT7A have a significantly shorter survival (Figure 5F). Since WNT7A is a known inducer of the WNT/β-catenin/TCF signaling cascade, we examined whether EVI1-induced WNT7A triggers canonical β-catenin signaling. When TCF-driven luciferase reporter plasmid was transfected into KPC-2D cells, we found that constitutive or induced EVI1 overexpression increases luciferase activity >2-fold (Figure 5G; Supplementary Figure S5C). As our findings suggest that WNT7A transactivated by EVI1 is functional, we attempted to address whether ectopic WNT7A expression can rescue phenotypic consequences of EVI1 deficiency. Since we observed marked changes of anchorage-independent growth and migration upon EVI1 knockdown, we tested the consequence of WNT7A restoration in these settings. Ectopic WNT7A expression can rescue, at least in part, impaired anchorage-independent growth and migration upon EVI1 depletion (Figure 5H and I; Supplementary Figure S5D and E). The partial rescue phenotype of WNT7A indicates that multiple targets of EVI1 pathway are likely to support aggressive PDA cells. Nonetheless, our findings indicate that the EVI1–WNT7A axis plays a key role in the transcription regulation of PDA malignancy.

## DISCUSSION

In this study, we have shown that PDA cells upregulate DNA binding protein EVI1, and EVI1 upregulation sup-

ports pro-tumorigenic phenotypes in PDA cells in a manner that requires SE activity. By examining public datasets, such as clinical and single-cell transcriptome information derived from patient samples, we identify that the EVI1 overexpression is associated with unfavorable clinical outcomes of PDA patients. We investigate the role of EVI1 in PDA using a combination of functional genomics, genetics and tumorigenesis assays, which lead us to conclude that EVI1 is an oncogenic TF installing tumor-intrinsic gene expression programs in PDA. To our knowledge, this is the first study that defines the chromatin regulatory function of EVI1 and reveals EVI1 as an attribute to the requirement of tumorigenesis in solid tumors.

While comprehensive genomic profiling has identified frequently mutated genes in PDA, most of them are not actionable drug targets (47). This challenge had guided us to focus on epigenetic traits of PDA. In a prior study, we implicated that FOXA1-driven enhancer reprogramming leads to a metastatic transition in PDA (10). A few chromatin regulators and TFs have been shown to determine molecular subtypes in PDA, including KDM6A, p63, ZBED2, GATA6 and HNF4 (7,8,19,48,49). Interestingly, a recent study raised the possibility that linked changes of genetic and epigenetic alterations attribute to PDA development (50). In this work, Morris *et al*. showed that p53 deficiency in PDA cells led to the accumulation of α-ketoglutarate, an essential metabolite for DNA and histone demethylase activity (50). In contrast, mutant p53 protein has been proposed to activate transcription of histone methyltransferase family genes, resulting in genome-wide changes of histone methylation landscape in cancers, including PDA (51). Alongside these pieces of evidence, our work highlights epigenetic contribution to PDA development.

It is important to compare findings in the current study with the prior research in which FOXA1-driven enhancer reprogramming was shown to promote PDA metastasis (10). The shared mechanism by which EVI1 and FOXA1 activate transcriptional reprogramming is acquiring H3K27ac and H3K4me1 marks on chromatin and requiring sustained TF expression to maintain active enhancers. At FOXA1-*GAIN* sites, where chromatin accessibility already presents without FOXA1 upregulation, FOXA1 perturbation does not affect nucleosome density. In contrast, the EVI1 level correlates with chromatin accessibility at EVI1-*GAIN* regions, indicating that EVI1-*GAIN* sites are not poised. Furthermore, EVI1-mediated chromatin accessibility likely starts the enhancer activation process, with subsequent enrichment of H3K4me1 and H3K27ac. Although most EVI1- and FOXA1-*GAIN* genomic regions are mutually exclusive, these TFs may reprogram the enhancer landscape in a concerted fashion. In line with our hypothesis, each of these TFs controls the developmental process, FOXA1 controls the lineage specification during embryogenesis (52) and EVI1 is vital for the embryonic developmental process (53). Therefore, it will be important to determine the synergistic effect of EVI1 and FOXA1 in PDA development.

One unexpected finding from our study is that EVI expression increases chromatin accessibility at EVI1-*GAIN* regions, preceding stereotypical histone modifications of an active enhancer. Altering inaccessible chromatin to accessible is a known property of pioneer TF and is required for initiating active transcription by recruiting other TFs, nucleosome remodelers and histone modifiers (54). So far, <20 TFs are known to possess such pioneering activity, and EVI1 was not among them (55). A simple scenario is that EVI1 may have an intrinsic pioneer function to scan DNA with inaccessible chromatin. However, it is more likely that EVI1 is assisted by physically interacting partners to indirectly open chromatin. Supporting such hypothesis, nuclear factor I family B (NFIB) was shown to increase chromatin accessibility in small cell lung cancer despite that NFIB is not a classical pioneer factor (56,57). Grabowska *et al*. showed that NFI family TFs can bind to pioneer TF FOXA1 in prostate cancer cells and suggested that NFIB could establish a pioneer function through interaction with a canonical pioneer factor (58). Bard-Chapeau *et al*. purified a large protein complex of EVI1 (59). Interestingly, from a total of 78 EVI1-interacting proteins, we found several components of ATP-dependent BRG1/BRM-associated factor (BAF) complex, including ARDI1B, SMARCA4, SMARCA5, SMARCC2 and SMARCE1. Because the BAF complex remodels chromatin by regulating chromatin accessibility (60,61), EVI1 can likely increase chromatin accessibility via the BAF complex. Supporting this hypothesis, SMARCA4, a core member of the BAF complex with ATPase activity, physically interacts with EVI1 and is critical for EVI1's oncogenic function (62).

Prior studies have implicated a role for EVI1 as an oncogene in human cancer. EVI1 is overexpressed in ∼10% of adult myeloid leukemia resulting from chromosomal rearrangements and contributes to leukemia development (22). Gröschel *et al*. showed that the rearrangement of the GATA2 enhancer locus drives EVI1 overexpression, implicating the importance of transcriptional deregulation of EVI1 (63). Acute EVI1 overexpression in adult mice without chromosomal rearrangement induces leukemic transformation, supporting the strong oncogenic ability of EVI1 (25). Besides hematologic malignancy, EVI1 overexpression has been reported in epithelial cancers as well. For instance, immunohistochemical analysis revealed that EVI1 is strongly expressed in the nucleus of PDA cells while absent in normal pancreatic tissues (29). However, the molecular mechanism that leads to EVI1 overexpression remains unclear in solid tumors since there is no report of genomic changes of the EVI1 locus. To our knowledge, our study is the first to show that PDA development accompanies the acquisition of 2345 SEs, and these SEs include five enhancer regions correlating with EVI1 overexpression. Disease-related SE acquisition is a mechanism of EVI1 overexpression in PDA malignancy. Further studies will be required to investigate enhancer-dependent EVI1 upregulation in other solid tumors.

In pancreatic cancer, little mechanism explains the oncogenic function of EVI1. Tanaka *et al*. (29) proposed that EVI1 antagonizes microRNA-96 (miR-96) production, which binds and suppresses KRAS expression in pancreatic cancer cells. In our loss- and gain-of-function experiments conducted in mouse and human pancreatic cancer cells, however, we could not detect significant changes of KRAS expression upon EVI1 overexpression or depletion (data not shown). The same group has also proposed glypican-

1 (GPC1) as another target of miR-96 in pancreatic cancer cells (64). Interestingly, Melo *et al*. (65) suggest GPC1 as a biomarker for PDA early detection, although it remains unclear whether GPC1 accumulation has a causal role in PDA development. As highlighted in our study, EVI1 may confer diverse biological processes of PDA development. Our findings from *in vitro* migration assays and GO term analysis strongly suggest that EVI1 may play a role in PDA metastasis. While we proposed that establishing a tumor-intrinsic gene expression network requires EVI1, we cannot completely rule out the tumor microenvironment regulation. For example, our scRNA-seq analysis detects EVI1 expression in endothelial cells in pancreatic tissue (Supplementary Figure S1F). From this analysis, we found that more endothelial cells from tumor samples express EVI1 mRNA than from normal pancreatic tissue, suggesting the involvement of EVI1 in regulating tumor-associated blood vessel development.

Although the debate over the origin of PDAC remains, several studies have shown that preneoplastic cells result from acinar dedifferentiation and acquisition of duct-like state (66). In recent studies, a unique expression pattern of EVI1 has been detected in human dedifferentiated acinar cells, identified from bulk and single-cell transcriptome analyses (67,68). However, it is still unclear whether EVI1 is critical for initiating PDA since acinar dedifferentiation resulting from caerulein-induced acute pancreatitis was not impaired in EVI1 knockout mice (67). Nevertheless, according to our work, it is possible that aberrant EVI1 upregulation in acinar cells preferentially generates preneoplastic lesions and enhances PDA progression.

The present study demonstrated that the aberrant enhancer landscape drives EVI1 upregulation and subsequently activates tumor-promoting transcriptional enhancers in PDA cells. We have now established EVI1 as a master regulator of PDA from comprehensive epigenome analysis and suggest WNT7A as an important downstream target of the EVI1 pathway. Therefore, interfering EVI1–WNT7A regulatory axis may establish a new therapeutic strategy to control PDA malignancy, and possibly other types of cancers with aberrant EVI1 expression.

## DATA AVAILABILITY

The ChIP-seq, ATAC-seq and RNA-seq data reported in this study are available in the Gene Expression Omnibus (GEO) database under GSE166511. Previously deposited scRNA-seq data can be found in the GSA database: CRA001160. Previously deposited ChIP-seq and RNA-seq data can be found in the GEO under GSE99311. Previously deposited PDA patient microarray data can be found in the GEO under GSE15471, GSE16515 and GSE28735.

## SUPPLEMENTARY DATA

Supplementary Data are available at NAR Cancer Online.

## ACKNOWLEDGEMENTS

We thank members of the Roe laboratory for insightful discussion and suggestions throughout this study. We also thank Drs David A. Tuveson and Nabeel M. Bardeesy for kindly providing murine pancreatic cancer organoids and cell lines, respectively.

## FUNDING

Ministry of Science and ICT [NRF-2018R1C1B6003133 and NRF-2021R1A2C4001420 to J.-S.R.]; Yonsei University [2018-22-0051 to J.-S.R.]; Brain Korea 21 FOUR Program [to J.-S.R., J.Y., H.-B.Y. and H.-R.K.].
*Conflict of interest statement.* None declared.

## REFERENCES

1. Siegel,R.L., Miller,K.D. and Jemal,A. (2019) Cancer statistics, 2019. *CA Cancer J. Clin.*, **69**, 7–34.
2. TCGA. (2017) Integrated genomic characterization of pancreatic ductal adenocarcinoma. *Cancer Cell*, **32**, 185–203.
3. O'Bryan,J.P. (2019) Pharmacological targeting of RAS: recent success with direct inhibitors. *Pharmacol. Res.*, **139**, 503–511.
4. Waters,A.M. and Der,C.J. (2018) KRAS: the critical driver and therapeutic target for pancreatic cancer. *Cold Spring Harb. Perspect. Med.*, **8**, a031435.
5. Collisson,E.A., Sadanandam,A., Olson,P., Gibb,W.J., Truitt,M., Gu,S., Cooc,J., Weinkle,J., Kim,G.E., Jakkula,L. *et al.* (2011) Subtypes of pancreatic ductal adenocarcinoma and their differing responses to therapy. *Nat. Med.*, **17**, 500–503.
6. Bailey,P., Chang,D.K., Nones,K., Johns,A.L., Patch,A.M., Gingras,M.C., Miller,D.K., Christ,A.N., Bruxner,T.J., Quinn,M.C. *et al.* (2016) Genomic analyses identify molecular subtypes of pancreatic cancer. *Nature*, **531**, 47–52.
7. Somerville,T.D.D., Xu,Y., Miyabayashi,K., Tiriac,H., Cleary,C.R., Maia-Silva,D., Milazzo,J.P., Tuveson,D.A. and Vakoc,C.R. (2018) TP63-mediated enhancer reprogramming drives the squamous subtype of pancreatic ductal adenocarcinoma. *Cell Rep.*, **25**, 1741–1755.
8. Somerville,T.D.D., Xu,Y., Wu,X.S., Maia-Silva,D., Hur,S.K., de Almeida,L.M.N., Preall,J.B., Koo,P.K. and Vakoc,C.R. (2020) ZBED2 is an antagonist of interferon regulatory factor 1 and modifies cell identity in pancreatic cancer. *Proc. Natl Acad. Sci. U.S.A.*, **117**, 11471–11482.
9. Goossens,S., Vandamme,N., Van Vlierberghe,P. and Berx,G. (2017) EMT transcription factors in cancer development re-evaluated: beyond EMT and MET. *Biochim. Biophys. Acta Rev. Cancer*, **1868**, 584–591.
10. Roe,J.S., Hwang,C.I., Somerville,T.D.D., Milazzo,J.P., Lee,E.J., Da Silva,B., Maiorino,L., Tiriac,H., Young,C.M., Miyabayashi,K. *et al.* (2017) Enhancer reprogramming promotes pancreatic cancer metastasis. *Cell*, **170**, 875–888.
11. Milan,M., Balestrieri,C., Alfarano,G., Polletti,S., Prosperini,E., Spaggiari,P., Zerbi,A., Diaferia,G.R. and Natoli,G. (2019) FOXA2 controls the *cis*-regulatory networks of pancreatic cancer cells in a differentiation grade-specific manner. *EMBO J.*, **38**, e102161.
12. Whyte,W.A., Orlando,D.A., Hnisz,D., Abraham,B.J., Lin,C.Y., Kagey,M.H., Rahl,P.B., Lee,T.I. and Young,R.A. (2013) Master transcription factors and mediator establish super-enhancers at key cell identity genes. *Cell*, **153**, 307–319.
13. Hnisz,D., Abraham,B.J., Lee,T.I., Lau,A., Saint-Andre,V., Sigova,A.A., Hoke,H.A. and Young,R.A. (2013) Super-enhancers in the control of cell identity and disease. *Cell*, **155**, 934–947.
14. Pott,S. and Lieb,J.D. (2015) What are super-enhancers? *Nat. Genet.*, **47**, 8–12.
15. Tang,F., Yang,Z., Tan,Y. and Li,Y. (2020) Super-enhancer function and its application in cancer targeted therapy. *NPJ Precis. Oncol.*, **4**, 2.
16. He,Y., Long,W. and Liu,Q. (2019) Targeting super-enhancers as a therapeutic strategy for cancer treatment. *Front. Pharmacol.*, **10**, 361.
17. McDonald,O.G., Li,X., Saunders,T., Tryggvadottir,R., Mentch,S.J., Warmoes,M.O., Word,A.E., Carrer,A., Salz,T.H., Natsume,S. *et al.* (2017) Epigenomic reprogramming during pancreatic cancer progression links anabolic glucose metabolism to distant metastasis. *Nat. Genet.*, **49**, 367–376.

18. Kalisz,M., Bernardo,E., Beucher,A., Maestro,M.A., Del Pozo,N., Millan,I., Haeberle,L., Schlensog,M., Safi,S.A., Knoefel,W.T. *et al.* (2020) HNF1A recruits KDM6A to activate differentiated acinar cell programs that suppress pancreatic cancer. *EMBO J.*, **39**, e102808.
19. Andricovich,J., Perkail,S., Kai,Y., Casasanta,N., Peng,W. and Tzatsos,A. (2018) Loss of KDM6A activates super-enhancers to induce gender-specific squamous-like pancreatic cancer and confers sensitivity to BET inhibitors. *Cancer Cell*, **33**, 512–526.
20. Hamdan,F.H. and Johnsen,S.A. (2018) DeltaNp63-dependent super enhancers define molecular identity in pancreatic cancer by an interconnected transcription factor network. *Proc. Natl Acad. Sci. U.S.A.*, **115**, E12343–E12352.
21. Noel,P., Hussein,S., Ng,S., Antal,C.E., Lin,W., Rodela,E., Delgado,P., Naveed,S., Downes,M., Lin,Y. *et al.* (2020) Triptolide targets super-enhancer networks in pancreatic cancer cells and cancer-associated fibroblasts. *Oncogenesis*, **9**, 100.
22. Nucifora,G. (1997) The EVI1 gene in myeloid leukemia. *Leukemia*, **11**, 2022–2031.
23. Bordereaux,D., Fichelson,S., Tambourin,P. and Gisselbrecht,S. (1990) Alternative splicing of the Evi-1 zinc finger gene generates mRNAs which differ by the number of zinc finger motifs. *Oncogene*, **5**, 925–927.
24. Glass,C., Wuertzer,C., Cui,X., Bi,Y., Davuluri,R., Xiao,Y.Y., Wilson,M., Owens,K., Zhang,Y. and Perkins,A. (2013) Global identification of EVI1 target genes in acute myeloid leukemia. *PLoS One*, **8**, e67134.
25. Ayoub,E., Wilson,M.P., McGrath,K.E., Li,A.J., Frisch,B.J., Palis,J., Calvi,L.M., Zhang,Y. and Perkins,A.S. (2018) EVI1 overexpression reprograms hematopoiesis via upregulation of Spi1 transcription. *Nat. Commun.*, **9**, 4239.
26. Deng,X., Cao,Y., Liu,Y., Li,F., Sambandam,K., Rajaraman,S., Perkins,A.S., Fields,A.P., Hellmich,M.R., Townsend,C.M. Jr *et al.* (2013) Overexpression of Evi-1 oncoprotein represses TGF-beta signaling in colorectal cancer. *Mol. Carcinog.*, **52**, 255–264.
27. Patel,J.B., Appaiah,H.N., Burnett,R.M., Bhat-Nakshatri,P., Wang,G., Mehta,R., Badve,S., Thomson,M.J., Hammond,S., Steeg,P. *et al.* (2011) Control of EVI-1 oncogene expression in metastatic breast cancer cells through microRNA miR-22. *Oncogene*, **30**, 1290–1301.
28. Nanjundan,M., Nakayama,Y., Cheng,K.W., Lahad,J., Liu,J., Lu,K., Kuo,W.L., Smith-McCune,K., Fishman,D., Gray,J.W. *et al.* (2007) Amplification of MDS1/EVI1 and EVI1, located in the 3q26.2 amplicon, is associated with favorable patient prognosis in ovarian cancer. *Cancer Res.*, **67**, 3074–3084.
29. Tanaka,M., Suzuki,H.I., Shibahara,J., Kunita,A., Isagawa,T., Yoshimi,A., Kurokawa,M., Miyazono,K., Aburatani,H., Ishikawa,S. *et al.* (2014) EVI1 oncogene promotes KRAS pathway through suppression of microRNA-96 in pancreatic carcinogenesis. *Oncogene*, **33**, 2454–2463.
30. Loven,J., Hoke,H.A., Lin,C.Y., Lau,A., Orlando,D.A., Vakoc,C.R., Bradner,J.E., Lee,T.I. and Young,R.A. (2013) Selective inhibition of tumor oncogenes by disruption of super-enhancers. *Cell*, **153**, 320–334.
31. Biankin,A.V., Waddell,N., Kassahn,K.S., Gingras,M.C., Muthuswamy,L.B., Johns,A.L., Miller,D.K., Wilson,P.J., Patch,A.M., Wu,J. *et al.* (2012) Pancreatic cancer genomes reveal aberrations in axon guidance pathway genes. *Nature*, **491**, 399–405.
32. Kottakis,F., Nicolay,B.N., Roumane,A., Karnik,R., Gu,H., Nagle,J.M., Boukhali,M., Hayward,M.C., Li,Y.Y., Chen,T. *et al.* (2016) LKB1 loss links serine metabolism to DNA methylation and tumorigenesis. *Nature*, **539**, 390–395.
33. Oni,T.E., Biffi,G., Baker,L.A., Hao,Y., Tonelli,C., Somerville,T.D.D., Deschenes,A., Belleau,P., Hwang,C.I., Sanchez-Rivera,F.J. *et al.* (2020) SOAT1 promotes mevalonate pathway dependency in pancreatic cancer. *J. Exp. Med.*, **217**, e20192389.
34. Klijn,C., Durinck,S., Stawiski,E.W., Haverty,P.M., Jiang,Z., Liu,H., Degenhardt,J., Mayba,O., Gnad,F., Liu,J. *et al.* (2015) A comprehensive transcriptional portrait of human cancer cell lines. *Nat. Biotechnol.*, **33**, 306–312.
35. Peran,I., Madhavan,S., Byers,S.W. and McCoy,M.D. (2018) Curation of the pancreatic ductal adenocarcinoma subset of the cancer genome atlas is essential for accurate conclusions about survival-related molecular mechanisms. *Clin. Cancer Res.*, **24**, 3813–3819.
36. Karamitopoulou,E. (2019) Tumour microenvironment of pancreatic cancer: immune landscape is dictated by molecular and histopathological features. *Br. J. Cancer*, **121**, 5–14.
37. Peng,J., Sun,B.F., Chen,C.Y., Zhou,J.Y., Chen,Y.S., Chen,H., Liu,L., Huang,D., Jiang,J., Cui,G.S. *et al.* (2019) Single-cell RNA-seq highlights intra-tumoral heterogeneity and malignant progression in pancreatic ductal adenocarcinoma. *Cell Res.*, **29**, 725–738.
38. Thomas-Chollier,M., Hufton,A., Heinig,M., O'Keeffe,S., Masri,N.E., Roider,H.G., Manke,T. and Vingron,M. (2011) Transcription factor binding predictions using TRAP for the analysis of ChIP-seq data and regulatory SNPs. *Nat. Protoc.*, **6**, 1860–1869.
39. Zuber,J., Shi,J., Wang,E., Rappaport,A.R., Herrmann,H., Sison,E.A., Magoon,D., Qi,J., Blatt,K., Wunderlich,M. *et al.* (2011) RNAi screen identifies Brd4 as a therapeutic target in acute myeloid leukaemia. *Nature*, **478**, 524–528.
40. Buenrostro,J.D., Giresi,P.G., Zaba,L.C., Chang,H.Y. and Greenleaf,W.J. (2013) Transposition of native chromatin for fast and sensitive epigenomic profiling of open chromatin, DNA-binding proteins and nucleosome position. *Nat. Methods*, **10**, 1213–1218.
41. Ashburner,M., Ball,C.A., Blake,J.A., Botstein,D., Butler,H., Cherry,J.M., Davis,A.P., Dolinski,K., Dwight,S.S., Eppig,J.T. *et al.* (2000) Gene Ontology: tool for the unification of biology. The Gene Ontology Consortium. *Nat. Genet.*, **25**, 25–29.
42. Gene Ontology Consortium. (2021) The Gene Ontology resource: enriching a GOld mine. *Nucleic Acids Res.*, **49**, D325–D334.
43. Long,H.K., Prescott,S.L. and Wysocka,J. (2016) Ever-changing landscapes: transcriptional enhancers in development and evolution. *Cell*, **167**, 1170–1187.
44. Catarino,R.R. and Stark,A. (2018) Assessing sufficiency and necessity of enhancer activities for gene expression and the mechanisms of transcription activation. *Genes Dev.*, **32**, 202–223.
45. Heintzman,N.D., Hon,G.C., Hawkins,R.D., Kheradpour,P., Stark,A., Harp,L.F., Ye,Z., Lee,L.K., Stuart,R.K., Ching,C.W. *et al.* (2009) Histone modifications at human enhancers reflect global cell-type-specific gene expression. *Nature*, **459**, 108–112.
46. GTEx Consortium. (2015) Human genomics. The Genotype-Tissue Expression (GTEx) pilot analysis: multitissue gene regulation in humans. *Science*, **348**, 648–660.
47. Lowery,M.A., Jordan,E.J., Basturk,O., Ptashkin,R.N., Zehir,A., Berger,M.F., Leach,T., Herbst,B., Askan,G., Maynard,H. *et al.* (2017) Real-time genomic profiling of pancreatic ductal adenocarcinoma: potential actionability and correlation with clinical phenotype. *Clin. Cancer Res.*, **23**, 6094–6100.
48. Adams,C.R., Htwe,H.H., Marsh,T., Wang,A.L., Montoya,M.L., Subbaraj,L., Tward,A.D., Bardeesy,N. and Perera,R.M. (2019) Transcriptional control of subtype switching ensures adaptation and growth of pancreatic cancer. *eLife*, **8**, e45313.
49. Brunton,H., Caligiuri,G., Cunningham,R., Upstill-Goddard,R., Bailey,U.M., Garner,I.M., Nourse,C., Dreyer,S., Jones,M., Moran-Jones,K. *et al.* (2020) HNF4A and GATA6 loss reveals therapeutically actionable subtypes in pancreatic cancer. *Cell Rep.*, **31**, 107625.
50. Morris,J.P.t., Yashinskie,J.J., Koche,R., Chandwani,R., Tian,S., Chen,C.C., Baslan,T., Marinkovic,Z.S., Sanchez-Rivera,F.J., Leach,S.D. *et al.* (2019) α-Ketoglutarate links p53 to cell fate during tumour suppression. *Nature*, **573**, 595–599.
51. Zhu,J., Sammons,M.A., Donahue,G., Dou,Z., Vedadi,M., Getlik,M., Barsyte-Lovejoy,D., Al-Awar,R., Katona,B.W., Shilatifard,A. *et al.* (2015) Gain-of-function p53 mutants co-opt chromatin pathways to drive cancer growth. *Nature*, **525**, 206–211.
52. Lee,C.S., Friedman,J.R., Fulmer,J.T. and Kaestner,K.H. (2005) The initiation of liver development is dependent on Foxa transcription factors. *Nature*, **435**, 944–947.
53. Yuasa,H., Oike,Y., Iwama,A., Nishikata,I., Sugiyama,D., Perkins,A., Mucenski,M.L., Suda,T. and Morishita,K. (2005) Oncogenic transcription factor Evi1 regulates hematopoietic stem cell proliferation through GATA-2 expression. *EMBO J.*, **24**, 1976–1987.
54. Zaret,K.S. (2020) Pioneer transcription factors initiating gene network changes. *Annu. Rev. Genet.*, **54**, 367–385.
55. Mayran,A. and Drouin,J. (2018) Pioneer transcription factors shape the epigenetic landscape. *J. Biol. Chem.*, **293**, 13795–13804.
56. Denny,S.K., Yang,D., Chuang,C.H., Brady,J.J., Lim,J.S., Gruner,B.M., Chiou,S.H., Schep,A.N., Baral,J., Hamard,C. *et al.*

(2016) Nfib promotes metastasis through a widespread increase in chromatin accessibility. *Cell*, **166**, 328–342.
57. Zaret,K.S. and Mango,S.E. (2016) Pioneer transcription factors, chromatin dynamics, and cell fate control. *Curr. Opin. Genet. Dev.*, **37**, 76–81.
58. Grabowska,M.M., Elliott,A.D., DeGraff,D.J., Anderson,P.D., Anumanthan,G., Yamashita,H., Sun,Q., Friedman,D.B., Hachey,D.L., Yu,X. *et al.* (2014) NFI transcription factors interact with FOXA1 to regulate prostate-specific gene expression. *Mol. Endocrinol.*, **28**, 949–964.
59. Bard-Chapeau,E.A., Gunaratne,J., Kumar,P., Chua,B.Q., Muller,J., Bard,F.A., Blackstock,W., Copeland,N.G. and Jenkins,N.A. (2013) EVI1 oncoprotein interacts with a large and complex network of proteins and integrates signals through protein phosphorylation. *Proc. Natl Acad. Sci. U.S.A.*, **110**, E2885–2894.
60. Narlikar,G.J., Sundaramoorthy,R. and Owen-Hughes,T. (2013) Mechanisms and functions of ATP-dependent chromatin-remodeling enzymes. *Cell*, **154**, 490–503.
61. Ho,L. and Crabtree,G.R. (2010) Chromatin remodelling during development. *Nature*, **463**, 474–484.
62. Chi,Y., Senyuk,V., Chakraborty,S. and Nucifora,G. (2003) EVI1 promotes cell proliferation by interacting with BRG1 and blocking the repression of BRG1 on E2F1 activity. *J. Biol. Chem.*, **278**, 49806–49811.
63. Groschel,S., Sanders,M.A., Hoogenboezem,R., de Wit,E., Bouwman,B.A.M., Erpelinck,C., van der Velden,V.H.J., Havermans,M., Avellino,R., van Lom,K. *et al.* (2014) A single oncogenic enhancer rearrangement causes concomitant EVI1 and GATA2 deregulation in leukemia. *Cell*, **157**, 369–381.
64. Tanaka,M., Ishikawa,S., Ushiku,T., Morikawa,T., Isagawa,T., Yamagishi,M., Yamamoto,H., Katoh,H., Takeshita,K., Arita,J. *et al.* (2017) EVI1 modulates oncogenic role of GPC1 in pancreatic carcinogenesis. *Oncotarget*, **8**, 99552–99566.
65. Melo,S.A., Luecke,L.B., Kahlert,C., Fernandez,A.F., Gammon,S.T., Kaye,J., LeBleu,V.S., Mittendorf,E.A., Weitz,J., Rahbari,N. *et al.* (2015) Glypican-1 identifies cancer exosomes and detects early pancreatic cancer. *Nature*, **523**, 177–182.
66. Storz,P. (2017) Acinar cell plasticity and development of pancreatic ductal adenocarcinoma. *Nat. Rev. Gastroenterol. Hepatol.*, **14**, 296–304.
67. Backx,E., Wauters,E., Baldan,J., Van Bulck,M., Michiels,E., Heremans,Y., De Paep,D.L., Kurokawa,M., Goyama,S., Bouwens,L. *et al.* (2021) MECOM permits pancreatic acinar cell dedifferentiation avoiding cell death under stress conditions. *Cell Death Differ.*, https://doi.org/10.1038/s41418-021-00771-6.
68. Wu,C., Chen,Z., Zhang,L., Zhu,Y., Deng,M., Huang,C., Liu,Y., Zhu,Q. and Wang,L. (2021) Sodium butyrate ameliorates deoxycorticosterone acetate/salt-induced hypertension and renal damage by inhibiting the MR/SGK1 pathway. *Hypertens. Res.*, **44**, 168–178.